NANO LETTERS

Letter

pubs.acs.org/NanoLett

Elastic Properties of Chemical-Vapor-Deposited Monolayer MoS_2, WS_2, and Their Bilayer Heterostructures

Kai Liu,[†,‡] Qimin Yan,[§,∥] Michelle Chen,[†] Wen Fan,[†,⊥] Yinghui Sun,[∥] Joonki Suh,[†] Deyi Fu,[†] Sangwook Lee,[†] Jian Zhou,[†] Sefaattin Tongay,[†] Jie Ji,[⊥] Jeffrey B. Neaton,[§,∥,#] and Junqiao Wu*[,†,‡]

[†]Department of Materials Science and Engineering, University of California, Berkeley, California 94720, United States

[‡]Materials Sciences Division and [§]Molecular Foundry, Lawrence Berkeley National Laboratory, Berkeley, California 94720, United States

[∥]Department of Physics, University of California, Berkeley, California 94720, United States

[⊥]Department of Thermal Science and Energy Engineering, University of Science and Technology of China, Anhui 230027, China

[#]Kavli Energy Nanosciences Institute, University of California, Berkeley, California 94720, United States

Supporting Information

ABSTRACT: Elastic properties of materials are an important factor in their integration in applications. Chemical vapor deposited (CVD) monolayer semiconductors are proposed as key components in industrial-scale flexible devices and building blocks of two-dimensional (2D) van der Waals heterostructures. However, their mechanical and elastic properties have not been fully characterized. Here we report high 2D elastic moduli of CVD monolayer MoS_2 and WS_2 (~170 N/m), which is very close to the value of exfoliated MoS_2 monolayers and almost half the value of the strongest material, graphene. The 2D moduli of their bilayer heterostructures are lower than the sum of 2D modulus of each layer but comparable to the corresponding bilayer homostructure, implying similar interactions between the hetero monolayers as between homo monolayers. These results not only provide deep insight into understanding interlayer interactions in 2D van der Waals structures but also potentially allow engineering of their elastic properties as desired.

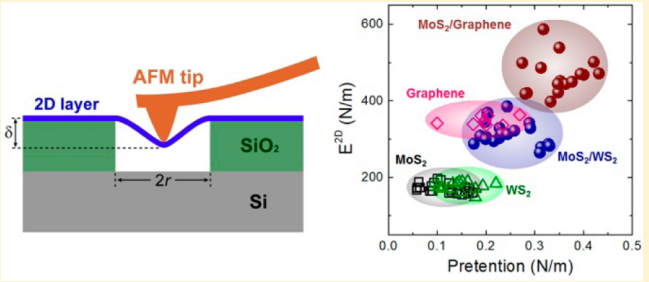

KEYWORDS: *Molybdenum disulfide, tungsten disulfide, monolayer, elastic modulus, heterostructures*

Two-dimensional (2D) semiconducting transition metal dichalcogenides (TMDs), such as MoS_2 and WS_2,[1,2] receive growing attention owing to their bandgap crossover from indirect in the bulk to direct in the monolayer[3−6] and a range of potential applications in optoelectronic and photonic devices.[7−9] Chemical vapor deposition (CVD) has been developed to synthesize low-cost and scalable 2D TMD monolayers for practical device applications.[10−14] It is also proposed as the most feasible approach to fabricate 2D heterostructures at industrial scale by simply stacking CVD-grown monolayers.[15] The diversity of 2D crystals results in a large number of possible 2D heterostructures that possess interesting charge-splitting functions for applications.[15−19] However, in contrast to their extensively studied electrical and optical properties, elastic and mechanical properties of 2D TMDs and their heterostructures have not been well characterized.

Elastic modulus is a basic parameter to determine mechanical properties of materials and is of vital importance in recent applications of flexible and stretchable electronics and photonics.[20] The 2D crystals have already been employed as key components in flexible devices due to their atomic thickness and ultrahigh flexibility.[21−24] However, reports on elastic properties of 2D TMDs are limited to less-defective, exfoliated MoS_2 with scattered experimental results,[25−27] while CVD-grown 2D TMDs have not been measured. On the other hand, interlayer coupling of 2D heterostructures plays a great role in the performance of devices. Although the coupling has been investigated electrically and optically in various 2D heterostructures,[15−19] a mechanical probing of the interlayer coupling is complementary but currently lacking.

In this work, we measured the elastic modulus of CVD-grown monolayer MoS_2 and WS_2 and probed the interlayer interaction of their heterostructures. The CVD-grown MoS_2 and WS_2 are found to have similarly high 2D elastic modulus, ~170 N/m, very close to the value of exfoliated MoS_2, and almost half of that of graphene. Theoretical simulations confirm that MoS_2 and WS_2 have nearly the same lattice constants and elastic properties. The 2D moduli of heterostructures are slightly lower than the sum of 2D modulus of each layer but

Received: May 14, 2014
Revised: July 30, 2014

dx.doi.org/10.1021/nl501793a | *Nano Lett.* XXXX, XXX, XXX−XXX

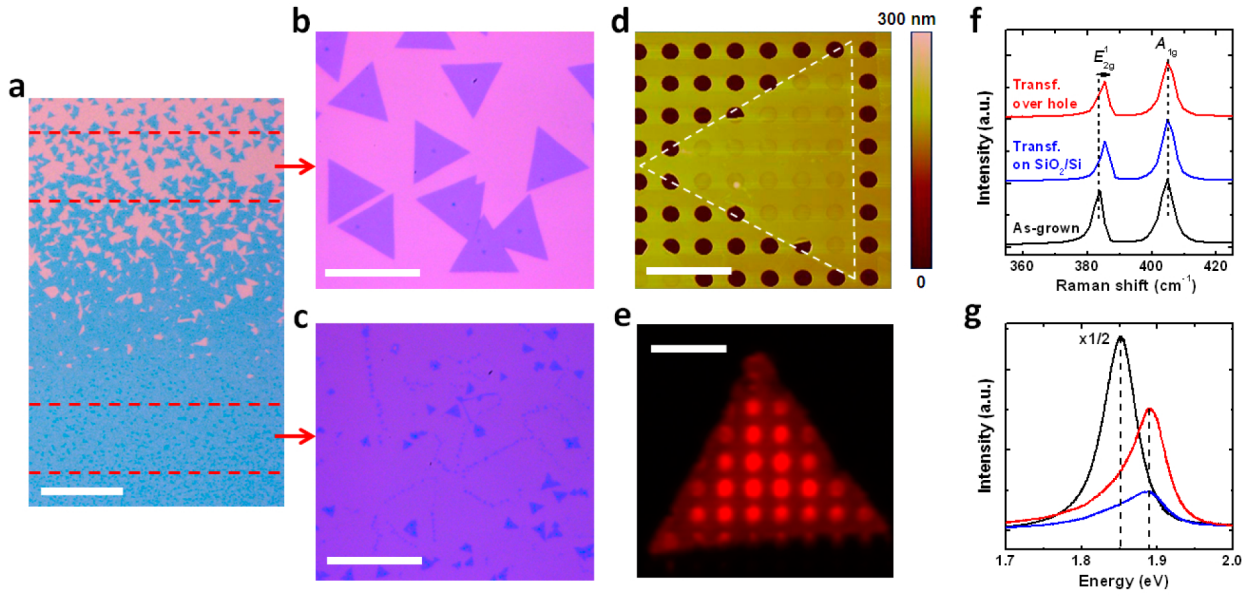

Figure 1. As-grown and transferred MoS_2 monolayer. (a) MoS_2 monolayer as grown on substrate, consisting of (b) isolated triangles and (c) continuous film of monolayers. (d) AFM topography of a triangle monolayer transferred onto the holey substrate. (e) Map of PL peak intensity from a triangle monolayer sitting on the holey substrate. (f,g) Raman and PL spectra of as-grown MoS_2, transferred MoS_2 in contact with SiO_2/Si, and suspended MoS_2 over holes. Scale bars: (a) 100 μm, (b,c) 10 μm, and (d,e) 5 μm.

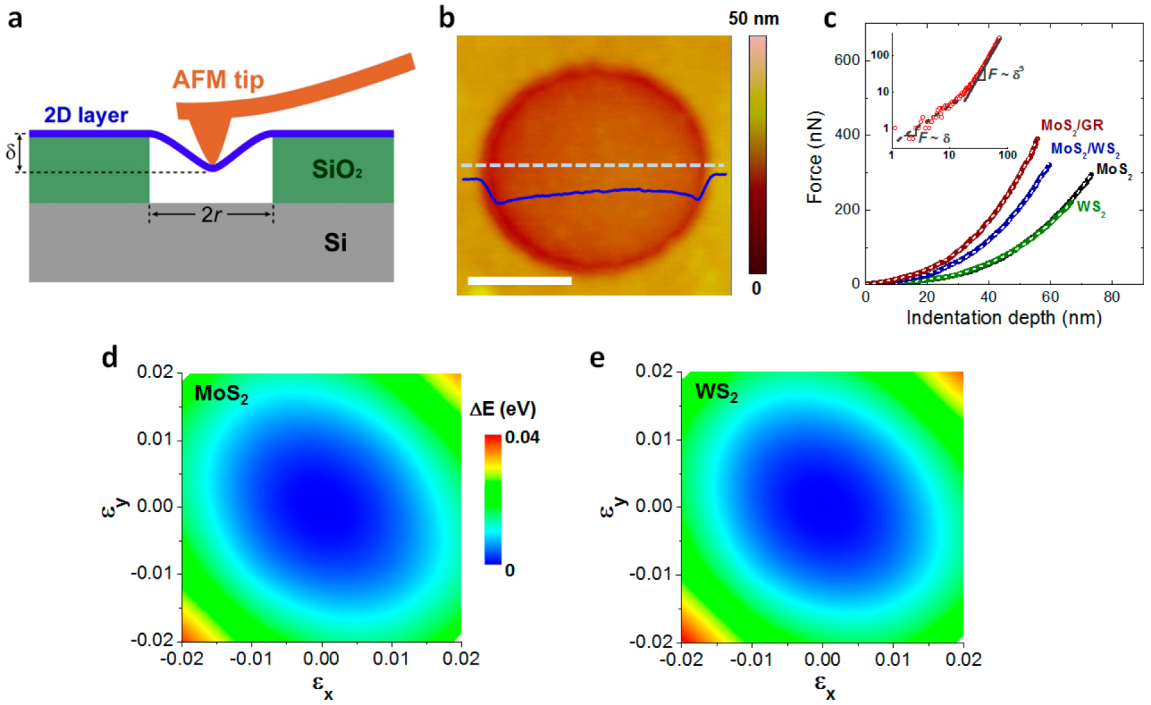

Figure 2. Elastic properties of 2D monolayers and heterostructures. (a) Illustration of the indentation measurement. (b) Typical AFM topography of a MoS_2 monolayer over a hole. Scale bar: 500 nm. (c) Force−displacement curves of different CVD monolayers and heterostructures. The white dashed lines are fitted by eq 1. (d,e) Contour plot of calculated elastic energy change for MoS_2 and WS_2 monolayers, respectively, under various biaxial strains.

comparable to the corresponding bilayer homostructures, implying similar interactions between heteromonolayers compared to between homomonolayers. The interlayer coupling of different bilayer homo- or heterostructures is also qualitatively compared. These results provide useful insight into understanding interlayer interactions in 2D materials and their utilization in flexible devices.

Monolayer MoS_2 (WS_2) were synthesized by CVD on SiO_2 (300 nm thick)/Si substrates with solid MoO_3 (WO_3) and S as precursors, similar to the method published previously.[14] The as-grown samples (Figure 1a) show isolated triangles of monolayer crystals at positions on the substrate slightly far away from the precursors, while closer to the precursors these triangles merge into a continuous film. The average size of these triangles is 10−15 μm. A thicker-layer island usually sits at

dx.doi.org/10.1021/nl501793a | Nano Lett. XXXX, XXX, XXX−XXX

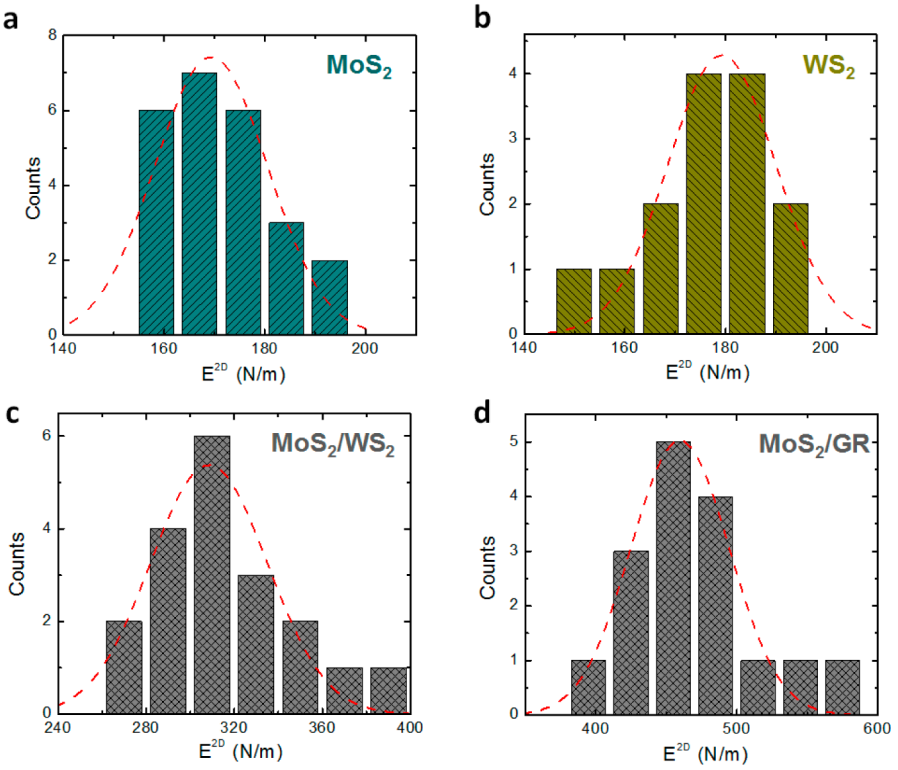

Figure 3. Histogram of E^{2D} for different 2D layers and heterostructures. (a) Triangles of CVD MoS_2. (b) CVD WS_2. (c) MoS_2/WS_2 heterostructure. (d) CVD MoS_2/exfoliated graphene heterostructure.

the center of each triangle (Figure 1b), which appears bigger and more evident in the continuous part (Figure 1c); this is probably due to the nucleation of additional layers over the bottom monolayer. The as-grown MoS_2 or WS_2 monolayers were then transferred onto a holey SiO_2/Si substrate by a polydimethylsiloxane (PDMS) stamping process (Supporting Information Figures S1 and S2). Figure 1d shows atomic force microscopy (AFM) image of a single MoS_2 monolayer triangle transferred onto the holey substrate. Photoluminescence (PL) mapping reveals a uniform light emission intensity from the MoS_2 monolayer in contact with the underneath SiO_2/Si substrate, while that of the suspended part over the holes is much brighter due to higher quantum yield (Figure 1e), consistent with the report on exfoliated monolayer MoS_2.[3]

For 2D crystals, Raman and PL spectra are typically utilized to distinguish the number of layers[28,29] as well as other effects such as strain and charge transfer.[30,31] As shown in Figure 1f, the out-of-plane Raman mode A_{1g} remains at ~405 cm^{-1}, but the in-plane mode E^1_{2g} blue shifts from 384 cm^{-1} in as-grown MoS_2 to ~386 cm^{-1} in transferred MoS_2. The separation between the E^1_{2g} and A_{1g} modes after the transfer is 19 cm^{-1}, similar to that of strain-free exfoliated monolayer MoS_2 (typically <20 cm^{-1}).[28,29] The PL of the as-grown sample shows a strong peak centered at ~1.85 eV, resulting from the A direct excitonic transition.[4] After the transfer, the PL intensity is dramatically reduced, and the PL peak is blue shifted to 1.89 eV (Figure 1g). The transfer of CVD WS_2 monolayers shows similar results (Supporting Information Figure S4). Both shifts of the PL and the in-plane Raman mode (E^1_{2g}) of the MoS_2 monolayer after the transfer can be attributed to the strain effect. It has been reported that a tensile strain softens PL and Raman modes of MoS_2 monolayer.[30] A similar strain may exist in as-grown MoS_2 monolayers due to the different thermal expansion coefficients of the materials in growth, and it will be released after the transfer such that the monolayer MoS_2 transferred is free of strain on the target substrate. The change of PL intensity may originate from the desorption/adsorption of molecules during the transfer.[31]

The elastic moduli of 2D layers are measured by indenting the center of the suspended part as a circular membrane with an AFM tip (Figure 2a). The tip is coated by diamond-like carbon and its diameter is ~20 nm. Tapping-mode AFM image displays that the 2D monolayer membranes are taut over the hole (Figure 2b). AFM images of bilayer homo- or heterostructures (Supporting Information Figure S5–S7) do not show evidence of bubbles or wrinkles either, whether on the substrate or over holes. This benefits from the dry PDMS stamping process, a technique proven capable of avoiding ripples or wrinkles that would introduce errors in measuring the modulus of CVD graphene.[32] For 2D materials, the strain energy is normalized by the sheet area, giving rise to 2D stress σ^{2D} and elastic modulus E^{2D}. MoS_2 and WS_2 have three-fold rotation symmetry and are thus isotropic in-plane. For such an ultrathin monolayer membrane clamped across a hole and indented at the center by a tiny tip ($r_{tip} \ll r_{hole}$), the bending modulus is negligible. The load is balanced by the pretension of the membrane and scales linearly with vertical deflection ($F \sim \delta$) under small loads.[33] When the load is large, it is dominated by the stiffness of the membrane with a cubic relationship, $F \sim \delta^3$ (inset of Figure 2c).[34] The force–displacement relationship can be described approximately as[35]

$$F = (\sigma_0^{2D}\pi)\delta + \left(E^{2D}\frac{q^3}{r^2}\right)\delta^3 \quad (1)$$

dx.doi.org/10.1021/nl501793a | Nano Lett. XXXX, XXX, XXX–XXX

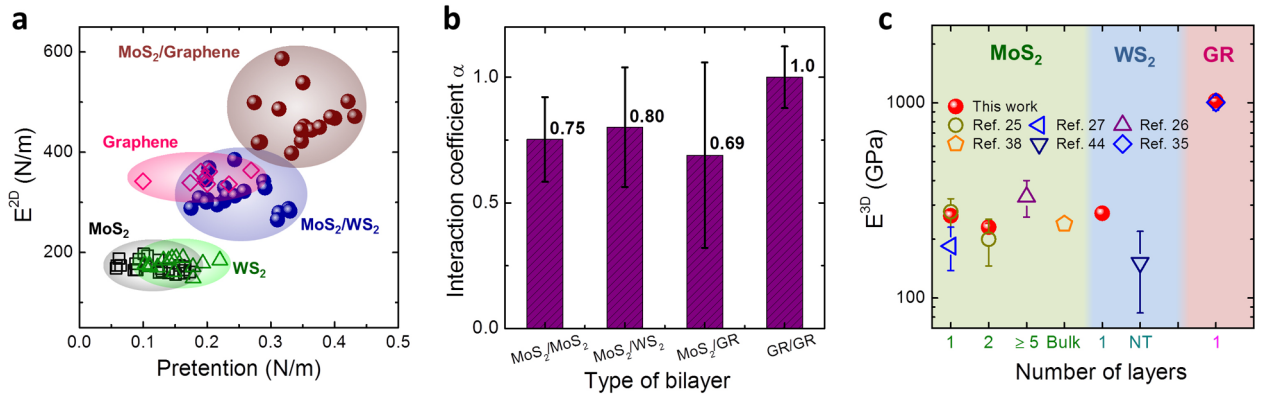

Figure 4. Comparison of elastic properties of different 2D layers. (a) Experimental data of 2D modulus and pretension for various 2D layers and heterostructures. (b) Interaction coefficients for different types of bilayers. (c) Comparison of Young's modulus of 2D monolayers with multilayers and bulk in the literature.

where F is the applied point load, δ is the indentation depth at the center of the membrane, σ_0^{2D} is the pretension, r is the radius of the hole, and q is a dimensionless constant determined by the Poisson's ratio (ν) of the membrane, obeying $q = 1/(1.05-0.15\nu - 0.16\nu^2)$. We utilized the values from first-principles calculations (details below), which are $\nu = 0.25$ and $\nu = 0.22$ for MoS_2 and WS_2, respectively, because of discrepancy in Poisson's ratios of MoS_2 in previous studies[25−27] and the lack of experimental value for WS_2 in literature. For graphene, $\nu = 0.165$.[35] σ_0^{2D} and E^{2D} can be derived by least-squares fitting of the experimental force−displacement data with eq 1 (Figure 2c).

To explore the elastic properties of monolayer MoS_2 and WS_2, we performed first-principles density functional theory calculations within the generalized gradient approximation (GGA) of Perdew, Burke, and Erzenhof (PBE),[36,37] using a plane-wave basis and the projector augmented wave (PAW) potentials as implemented in the VASP code. Details of calculation can be found in the Supporting Information Figure S8 and Methods. Figure 2d,e shows the contour plot of change in elastic energy as a function of strain along the x- and y-directions. The 2D elastic moduli and Poisson's ratios derived from the calculated data are 123 N/m and 0.25 for MoS_2 and 137 N/m and 0.22 for WS_2, respectively. The calculated Poisson's ratio of MoS_2 is close to the experimental value (~0.27 in ref 38), while the calculated value of WS_2 provides a reference for our experimental fitting of modulus as it has never been measured.

We measured 7−15 suspended circular membranes for each type of 2D layers (graphene, MoS_2, WS_2, and their heterostructures) and indented each membrane with 2−3 different applied forces. For bilayer heterostructures, q is taken as the average value of the two layers, because of the weak interlayer van der Waals interaction and the resultant difficulty in determining the Poisson's ratios of heterostructures from our calculations. On the other hand, the separate q values of MoS_2, WS_2, and graphene are very close to each other (0.998, 0.991, 0.980, respectively); therefore, an average value of q will not introduce significant errors for the fitting.

Figure 3 shows the statistical histogram of the 2D modulus of MoS_2, WS_2 monolayers, and their heterostructures, MoS_2/WS_2 and MoS_2/graphene. The 2D moduli are 171 ± 11 and 177 ± 12 N/m for MoS_2 and WS_2 (Figure 3a,b), respectively, where the values before ± are the average values and the errors are standard deviations of the measurements. These values are nearly half the value of graphene (349 ± 12 N/m in our experiment and ~340 N/m in literatures), which is the strongest 2D material.[32,35] The small difference in the modulus between MoS_2 and WS_2 is consistent with the calculation, although both experimental values are higher than the calculated values. This observation is consistent with the fact that DFT-GGA usually underestimates the bulk modulus of many traditional semiconductor materials.[39]

The 2D bilayer heterostructures were prepared by stacking different 2D layers in sequence (Supporting Information Figure S5 and S7). The moduli of MoS_2/WS_2 and MoS_2/graphene heterostructures are measured to be 314 ± 31 and 467 ± 48 N/m (Figure 3c,d), respectively, which are both lower than the summed modulus of the consisting layers (348 and 520 N/m, respectively). Figure 4a shows all the experimental data of σ_0^{2D} and E^{2D} for different 2D layers and heterostructures. The pretension of 2D layers depends not only on the transfer process but also on their intrinsic mechanical properties, because this parameter relates to the elastic energy of pretension after the transfer. Therefore, different monolayers or heterostructures can have different pretension values. The average pretensions are 0.11 ± 0.04, 0.15 ± 0.03, and 0.20 ± 0.05 N/m for monolayer MoS_2, WS_2, and graphene, respectively. The positive pretensions may originate from adhesion of the monolayer membrane to the sidewall of the hole (Figure 2b), also consistent with the reports on exfoliated graphene and MoS_2.[25,35] Interestingly, the pretensions of the heterostructures, MoS_2/WS_2 and MoS_2/graphene, are almost the summed pretension of both layers, which are 0.25 ± 0.05 and 0.35 ± 0.05 N/m, respectively. This indicates that the pretention is simply accumulated as the layers are stacked sequentially by the same transfer process.

The simple stacking process for fabricating heterostructures has a general concern that whether the van der Waals heterostructures have strong interlayer interaction. While optical and electrical methods investigate the electronic coupling that has a strong influence on band structure renormalization,[16,17] mechanical measurements can also probe the coupling force between the layers. In our experiments, none of the force−displacement curves of monolayers shows evidence of sliding (e.g., irreversible force−displacement dependence). Therefore, the bottom layer in direct contact with the substrate should be firmly clamped onto the substrate within the range of load applied. In the extreme case of very strong interlayer interactions in a bilayer structure, there is no

dx.doi.org/10.1021/nl501793a | Nano Lett. XXXX, XXX, XXX−XXX

interlayer sliding allowed, and both layers contribute to the 2D modulus measured with our method. In the opposite extreme, that is, in the absence of interaction between layers, the top layer is free to slide against the bottom layer, and the measured modulus of the bilayer is solely given by the bottom layer that is clamped by the substrate. Thus, the measured modulus of a 2D bilayer hetero- or homostructure can be phenomenologically described by

$$E^{2D}_{measured} = E^{2D}_{bottom} + \alpha E^{2D}_{top} \quad (2)$$

where $E^{2D}_{measured}$, E^{2D}_{bottom}, and E^{2D}_{top} are the 2D modulus of, respectively, the bilayer, the bottom layer, and the top layer, and the "interaction coefficient" α ranges from 0 to 1 describing the contribution of the top layer to the measured value. α may depend on the interlayer friction coefficient, the van der Waals interaction between layers, and the strain that relates to the indentation depth. The elastic strain can reach several percent in graphene or 2D semiconductors, but stacking faults or strain solitons observed in AB-stacked bilayer graphene may also exist in our randomly stacked 2D layers,[40] which might induce a nonlinear friction regime for small strains and render this interaction coefficient dependent on the strain. In our experiments, however, the measured E^{2D} at various indentation depths for all bilayer structures indicate that E^{2D} is independent of the indentation depth (Supporting Information Figure S9). This result suggests that the interaction coefficient does not depend on the strain in the system. Therefore, α can be used as a parameter to compare the interlayer coupling in different bilayer homo- or heterostructures.

Besides the nanoindentation, nanoscale shearing or telescopic sliding can also be used to measure the interlayer interaction in graphite[41] or in multiwalled nanotubes.[42,43] Compared to the nanoindentation, these methods provide a more direct way to quantify the interlayer friction. However, the nanoindentation is a relatively simple method to qualitatively compare the interlayer coupling in different bilayer structures. The lower effective modulus of MoS_2/WS_2 heterostructures compared to the consisting layers gives α = 0.80, which indicates that a slight interlayer sliding probably occurred between the MoS_2 and WS_2 layers during the measurement. We note that the 2D modulus of exfoliated bilayer MoS_2 was also reported to be lower than twice the value of the monolayer.[25] As a comparison, we also measured the modulus of exfoliated bilayer MoS_2 (Supporting Information Figure S6), which is 300 ± 13 N/m with α = 0.75 (Figure 4b). Because MoS_2 and WS_2 used in our experiments have nearly the same 2D modulus, this result suggests that the interaction between the MoS_2 and WS_2 layer is comparable to that in the bilayer MoS_2.

Among the various 2D van der Waals heterostructures, graphene/TMD has recently attracted much interest.[16−18] We have formed graphene/MoS_2 heterostructures by exfoliating monolayer graphene onto a holey substrate followed by stamping CVD MoS_2 (Supporting Information, Figure S7). We note that the 2D modulus of graphene depends very linearly on the number of layers (data not shown here), indicating a relatively strong interaction between graphene homolayers preventing interlayer sliding during the measurement, corresponding to an α value of almost 1 (Figure 4b). The MoS_2/graphene heterostructure, however, only gives rise to α = 0.69 (Figure 4b), indicating a moderately strong interaction.

In these atomic structures, 2D modulus is more intrinsic. However, the conversion of 2D to 3D modulus enables a comparison of the modulus of 2D layers with the conventional Young's modulus of bulk materials. For the layered materials, the bulk can be considered as the stacking of a large number of monolayers. The thickness of the bulk is determined by the number of the layers multiplied by the interlayer distance. Therefore, one needs to divide the 2D value of the monolayer by the interlayer distance in order to convert into the normal 3D Young's modulus and compare to each other. This is also the method used in literature to calculate the 3D modulus of graphene[35] and exfoliated monolayer MoS_2.[25] Figure 4c summarizes the Young's moduli of three types of 2D materials (MoS_2, WS_2, and graphene) obtained in this work as well as those reported in literature. The interlayer distance used is 0.34 nm for graphene and 0.65 nm for both MoS_2 and WS_2. The corresponding 3D modulus is 264 ± 18 GPa for MoS_2, 272 ± 18 GPa for WS_2, and 1025 ± 35 GPa for graphene. The modulus of CVD MoS_2 is consistent with the result of exfoliated MoS_2 monolayer (~270 GPa).[25] Both moduli of monolayer MoS_2 and WS_2 are higher than experimental values of bulk MoS_2 (~240 GPa)[38] and multilayer WS_2 nanotubes (~170 GPa),[44] which may suggest a dependence of the Young's modulus on the number of layers due to the interlayer sliding in multilayers or bulk.

In summary, we experimentally and theoretically investigated the elastic properties of CVD-grown MoS_2, WS_2, and their heterostructures. Our work not only quantifies the elastic modulus of these 2D structures but also defines an interaction coefficient between neighboring monolayers that measures the interlayer coupling. As interesting devices can be built from CVD 2D semiconductors and their heterostructures, our results provide calibrated values of their elastic modulus for various applications, especially in flexible electronic and mechanical devices. The studies of interlayer coupling provide a way to probe and understand electronic and mechanical coupling between monolayers in a variety of 2D structures.

Methods. *Synthesis of MoS_2 and WS_2.* MoS_2 and WS_2 monolayers were grown onto SiO_2/Si substrates using an ambient vapor transport technique. Prior to the growth, SiO_2/Si substrates were treated with Piranha solution for 2 h. Our results show that this step is critical to achieve clean, large single crystal domain and continuous area monolayers. After the piranha treatment, the samples were washed with DI water and dried using N_2 gas. Three milligrams of MoO_3 powder is loaded in the alumina crucible and the samples are placed facing down. MoO_3 source was placed downstream from the sulfur source at ~19 cm away from the sulfur containing crucible. The system was purged with ultrahigh purity N_2 gas with 500 sccm flow rate for 10 min and heated up to 300 °C for 10 min with 100 sccm. Sulfur source melted at 600 °C and S_2 gas was delivered to the growth zone at 2 sccm flow rate. The growth temperature was 690 °C for 3 min. During the cool down, S gas was kept at a constant rate (2−5 sccm) to avoid material deterioration. Below 590 °C, the flow is increased to 300 sccm for faster cooling down. WS_2 growth was the same as above but the growth temperature was set at 800 °C and the sulfur source was melted (introduced) only after 760 °C.

Transfer of 2D Materials and Their Heterostructures. The transfer process of monolayer TMDs is shown in the Supporting Information Figure S1. As-grown CVD MoS_2 or WS_2 monolayer coated SiO_2/Si substrate was cut into long narrow strips, attached to a PDMS film, and baked at 80 °C for

dx.doi.org/10.1021/nl501793a | Nano Lett. XXXX, XXX, XXX−XXX

1 h to ensure a good adhesion between the PDMS and the substrate. Then it was floated on 1 M KOH solution until the substrate was etched off. The cutting of long-strip samples could decrease etching time, which is only 1−2 h in our experiments. The left MoS_2/PDMS or WS_2/PDMS was rinsed in DI water for several times and then dried naturally. Afterward, MoS_2/PDMS or WS_2/PDMS was attached onto a holey substrate and kept there for ∼2 h. PDMS film was then peeled off slowly, leaving MoS_2 or WS_2 monolayers on the holey substrate. MoS_2/WS_2 heterostructure was fabricated by stamping first WS_2 and then MoS_2 with a control of overlapping both monolayer parts. To make a MoS_2/graphene heterostructure, a graphene monolayer was first exfoliated onto a holey substrate, and then CVD MoS_2 monolayer was located and stamped onto the graphene monolayer.

PDMS residues may reduce the interlayer interaction in the heterostructures. In our experiments, the KOH etching time and the PDMS attaching time on the target substrate are optimized to reduce the PDMS residues as much as possible. After the transfer, small PDMS particles were found occasionally to leave on some monolayers in AFM images. However, these particles distributed sparsely and occupied only a very small fraction of the whole 2D area. Therefore, the reduction of the interlayer interaction due to the PDMS residues was low and negligible and did not introduce large errors in the measurements.

Measurement of Modulus. Holey substrates were fabricated by a deep UV photolithography followed by a deep reactive ion etching. The size of circular holes is diameter = 1.1 μm and depth = 0.3 μm. To measure elastic properties of 2D layers, a force (200−450 nN) was applied at the center of the suspended circular membranes through an AFM (Veeco Multimode) tip. The tip is coated by diamond-like carbon and its diameter is ∼20 nm (μmasch, HQ: NSC15).The indentation depth, δ, was determined by $\Delta z_{piezo} - \Delta z_{tip}$, where Δz_{piezo} is the displacement of the scanning piezo-tube of AFM and Δz_{tip} is the deflection of the AFM tip. The spring constant of the tip is 43.8 N/m, which was calibrated by a reference cantilever. All of the samples in this work, including monolayers and heterostructures, were measured by the same AFM tip to avoid errors introduced by using different tips.

Calculation of Modulus. In our DFT calculations within the GGA using the PBE function, we used a 9 × 9 × 2 Γ-point centered *k*-point mesh to sample the Brillouin zone and a plane-wave cutoff of 500 eV. The single-layer structures were simulated with supercells, including as much as 12 Å of vacuum to avoid the interaction between monolayers in neighboring cells, and periodic boundary conditions. All atomic positions were fully optimized and the maximum Hellmann−Feynman forces on each atom were less than 0.01 eV/Å. The unit cell and *x*−*y* directions are shown in Supporting Information Figure S8. Our calculated unit cell parameters were nearly the same for MoS_2 (a = 3.190 nm) and WS_2 (a = 3.191 nm). Small strains were applied along *x*- and *y*-directions, and total energies were calculated and fitted with the formula $E_s = a_1\varepsilon_x^2 + a_2\varepsilon_y^2 + a_3\varepsilon_x\varepsilon_y$ using a least-squares method. Here E_s is the energy deviation of the strained system from the equilibrium unstrained system, and ε_x and ε_y are the strain applied in *x*- and *y*-directions, respectively. Because of the isotropy of honeycomb lattice, a_1 equals a_2. The coefficients determined the elastic modulus Y and Poisson's ratio ν, following $Y = (2a_1 - a_3^2/2a_1)/A_0$ and $\nu = a_3/2a_1$, where A_0 is the area of the unit cell.[36,37]

■ ASSOCIATED CONTENT

Supporting Information

Transfer process of monolayer MoS_2 and WS_2, MoS_2 monolayers transferred on a holey substrate, comparison of isolated and continuous parts of CVD MoS_2 monolayers, as-grown and as-transferred WS_2, MoS_2/WS_2 heterostructure, exfoliated MoS_2 bilayer, MoS_2/graphene heterostructure, model for the calculation of elastic properties of MoS_2 and WS_2, and E^{2D} at various indentation depths. This material is available free of charge via the Internet at http://pubs.acs.org.

■ AUTHOR INFORMATION

Corresponding Author

*E-mail: wuj@berkeley.edu.

Notes

The authors declare no competing financial interest.

■ ACKNOWLEDGMENTS

This work was supported by the Office of Science, Office of Basic Energy Sciences, of the U.S. Department of Energy under Contract No. DE-AC02-05CH11231.The AFM characterization was partially supported by the NSF Center for Energy Efficient Electronics Science (NSF Award No. ECCS-0939514). The computational part of this work is supported by the U.S. Department of Energy, Office of Basic Energy Sciences, Materials Sciences and Engineering Division, under Contract No. DE-AC02-05CH11231. Portions of the computation work were done using NERSC resources. We thank Cong Liu for assistance in fabricating the holey substrates.

■ REFERENCES

(1) Wang, Q. H.; Kalantar-Zadeh, K.; Kis, A.; Coleman, J. N.; Strano, M. S. *Nat. Nanotechnol.* **2012**, *7* (11), 699−712.
(2) Butler, S. Z.; Hollen, S. M.; Cao, L. Y.; Cui, Y.; Gupta, J. A.; Gutiérrez, H. R.; Heinz, T. F.; Hong, S. S.; Huang, J. X.; Ismach, A. F.; Johnston-Halperin, E.; Kuno, M.; Plashnitsa, V. V.; Robinson, R. D.; Ruoff, R. S.; Salahuddin, S.; Shan, J.; Shi, L.; Spencer, M. G.; Terrones, M.; Windl, W.; Goldberger, J. E. *ACS Nano* **2013**, *7* (4), 2898−2926.
(3) Mak, K. F.; Lee, C.; Hone, J.; Shan, J.; Heinz, T. F. *Phys. Rev. Lett.* **2010**, *105* (13), 136805.
(4) Splendiani, A.; Sun, L.; Zhang, Y. B.; Li, T. S.; Kim, J.; Chim, C. Y.; Galli, G.; Wang, F. *Nano Lett.* **2010**, *10* (4), 1271−1275.
(5) Zhang, Y.; Chang, T. R.; Zhou, B.; Cui, Y. T.; Yan, H.; Liu, Z. K.; Schmitt, F.; Lee, J.; Moore, R.; Chen, Y. L.; Lin, H.; Jeng, H. T.; Mo, S. K.; Hussain, Z.; Bansil, A.; Shen, Z. X. *Nat. Nanotechnol.* **2014**, *9* (2), 111−115.
(6) Jin, W.; Yeh, P.-C.; Zaki, N.; Zhang, D.; Sadowski, J. T.; Al-Mahboob, A.; van der Zande, A. M.; Chenet, D. A.; Dadap, J. I.; Herman, I. P.; Sutter, P.; Hone, J.; Osgood, R. M., Jr. *Phys. Rev. Lett.* **2013**, *111*, 106801.
(7) Lopez-Sanchez, O.; Lembke, D.; Kayci, M.; Radenovic, A.; Kis, A. *Nat. Nanotechnol.* **2013**, *8* (7), 497−501.
(8) Radisavljevic, B.; Radenovic, A.; Brivio, J.; Giacometti, V.; Kis, A. *Nat. Nanotechnol* **2011**, *6* (3), 147−150.
(9) Yoon, Y.; Ganapathi, K.; Salahuddin, S. *Nano Lett.* **2011**, *11* (9), 3768−3773.
(10) Lee, Y. H.; Zhang, X. Q.; Zhang, W. J.; Chang, M. T.; Lin, C. T.; Chang, K. D.; Yu, Y. C.; Wang, J. T. W.; Chang, C. S.; Li, L. J.; Lin, T. W. *Adv. Mater.* **2012**, *24* (17), 2320−2325.
(11) Liu, K. K.; Zhang, W. J.; Lee, Y. H.; Lin, Y. C.; Chang, M. T.; Su, C. Y.; Chang, C. S.; Li, H.; Shi, Y. M.; Zhang, H.; Lai, C. S.; Li, L. J. *Nano Lett.* **2012**, *12* (3), 1538−1544.
(12) Najmaei, S.; Liu, Z.; Zhou, W.; Zou, X. L.; Shi, G.; Lei, S. D.; Yakobson, B. I.; Idrobo, J. C.; Ajayan, P. M.; Lou, J. *Nat. Mater.* **2013**, *12* (8), 754−759.

(13) Shi, Y. M.; Zhou, W.; Lu, A. Y.; Fang, W. J.; Lee, Y. H.; Hsu, A. L.; Kim, S. M.; Kim, K. K.; Yang, H. Y.; Li, L. J.; Idrobo, J. C.; Kong, J. *Nano Lett.* **2012**, *12* (6), 2784−2791.
(14) van der Zande, A. M.; Huang, P. Y.; Chenet, D. A.; Berkelbach, T. C.; You, Y. M.; Lee, G. H.; Heinz, T. F.; Reichman, D. R.; Muller, D. A.; Hone, J. C. *Nat. Mater.* **2013**, *12* (6), 554−561.
(15) Geim, A. K.; Grigorieva, I. V. *Nature* **2013**, *499* (7459), 419−425.
(16) Yu, W. J.; Li, Z.; Zhou, H. L.; Chen, Y.; Wang, Y.; Huang, Y.; Duan, X. F. *Nat. Mater.* **2013**, *12* (3), 246−252.
(17) Yu, W. J.; Liu, Y.; Zhou, H. L.; Yin, A. X.; Li, Z.; Huang, Y.; Duan, X. F. *Nat. Nanotechnol.* **2013**, *8* (12), 952−958.
(18) Britnell, L.; Ribeiro, R. M.; Eckmann, A.; Jalil, R.; Belle, B. D.; Mishchenko, A.; Kim, Y. J.; Gorbachev, R. V.; Georgiou, T.; Morozov, S. V.; Grigorenko, A. N.; Geim, A. K.; Casiraghi, C.; Neto, A. H. C.; Novoselov, K. S. *Science* **2013**, *340* (6138), 1311−1314.
(19) Tongay, S.; Fan, W.; Kang, J.; Park, J.; Koldemir, U.; Suh, J.; Narang, D. S.; Liu, K.; Ji, J.; Li, J.; Sinclair, R.; Wu, J. *Nano Lett.* **2014**, *14* (6), 3185−3190.
(20) Rogers, J. A.; Someya, T.; Huang, Y. G. *Science* **2010**, *327* (5973), 1603−1607.
(21) He, Q. Y.; Zeng, Z. Y.; Yin, Z. Y.; Li, H.; Wu, S. X.; Huang, X.; Zhang, H. *Small* **2012**, *8* (19), 2994−2999.
(22) Pu, J.; Yomogida, Y.; Liu, K. K.; Li, L. J.; Iwasa, Y.; Takenobu, T. *Nano Lett.* **2012**, *12* (8), 4013−4017.
(23) Chang, H. Y.; Yang, S. X.; Lee, J. H.; Tao, L.; Hwang, W. S.; Jena, D.; Lu, N. S.; Akinwande, D. *ACS Nano* **2013**, *7* (6), 5446−5452.
(24) Salvatore, G. A.; Munzenrieder, N.; Barraud, C.; Petti, L.; Zysset, C.; Buthe, L.; Ensslin, K.; Troster, G. *ACS Nano* **2013**, *7* (10), 8809−8815.
(25) Bertolazzi, S.; Brivio, J.; Kis, A. *ACS Nano* **2012**, *5* (12), 9703−9709.
(26) Castellanos-Gomez, A.; Poot, M.; Steele, G. A.; van der Zant, H. S.; Agrait, N.; Rubio-Bollinger, G. *Adv. Mater.* **2012**, *24* (6), 772−775.
(27) Cooper, R. C.; Lee, C.; Marianetti, C. A.; Wei, X.; Hone, J.; Kysar, J. W. *Phys. Rev. B* **2013**, *87*, 035423.
(28) Lee, C.; Yan, H.; Brus, L. E.; Heinz, T. F.; Hone, J.; Ryu, S. *ACS Nano* **2010**, *4* (5), 2695−2700.
(29) Li, H.; Zhang, Q.; Yap, C. C. R.; Tay, B. K.; Edwin, T. H. T.; Olivier, A.; Baillargeat, D. *Adv. Funct. Mater.* **2012**, *22* (7), 1385−1390.
(30) Conley, H. J.; Wang, B.; Ziegler, J. I.; Haglund, R. F.; Pantelides, S. T.; Bolotin, K. I. *Nano Lett.* **2013**, *13* (8), 3626−3630.
(31) Tongay, S.; Zhou, J.; Ataca, C.; Liu, J.; Kang, J. S.; Matthews, T. S.; You, L.; Li, J.; Grossman, J. C.; Wu, J. *Nano Lett.* **2013**, *13* (6), 2831−2836.
(32) Lee, G. H.; Cooper, R. C.; An, S. J.; Lee, S.; van der Zande, A.; Petrone, N.; Hammerberg, A. G.; Lee, C.; Crawford, B.; Oliver, W.; Kysar, J. W.; Hone, J. *Science* **2013**, *340* (6136), 1073−1076.
(33) Wan, K.-T.; Guo, S.; Dillard, D. A. *Thin Solid Films* **2003**, *425*, 150−162.
(34) Komaragiri, U.; Begley, M. R.; Simmonds, J. G. *J. Appl. Mech.* **2005**, *72* (2), 203−212.
(35) Lee, C.; Wei, X.; Kysar, J. W.; Hone, J. *Science* **2008**, *321* (5887), 385−388.
(36) Topsakal, M.; Cahangirov, S.; Ciraci, S. *Appl. Phys. Lett.* **2010**, *96* (9), 091912.
(37) Yue, Q.; Kang, J.; Shao, Z.; Zhang, X.; Chang, S.; Wang, G.; Qin, S.; Li, J. *Phys. Lett. A* **2012**, *376* (12−13), 1166−1170.
(38) Feldman, J. L. *J. Phys. Chem. Solids* **1976**, *37*, 1141−1144.
(39) Filippi, C.; Singh, D. J.; Umrigar, C. J. *Phys. Rev. B* **1994**, *50* (20), 14947−14951.
(40) Alden, J. S.; Tsen, A. W.; Huang, P. Y.; Hovden, R.; Brown, L.; Park, J.; Muller, D. A.; McEuen, P. L. *Proc. Natl. Acad. Sci. U.S.A.* **2013**, *110* (28), 11256−11260.
(41) Liu, Z.; Yang, J.; Grey, F.; Liu, J. Z.; Liu, Y.; Wang, Y.; Yang, Y.; Cheng, Y.; Zheng, Q. *Phys. Rev. Lett.* **2012**, *108*, 205503.
(42) Kis, A.; Jensen, K.; Aloni, S.; Mickelson, W.; Zettl, A. *Phys. Rev. Lett.* **2006**, *97*, 025501.
(43) Nigues, A.; Siria, A.; Vincent, P.; Poncharal, P.; Bocquet, L. *Nat. Mater.* **2014**, *13* (7), 688−693.
(44) Kaplan-Ashiri, I.; Cohen, S. R.; Gartsman, K.; Ivanovskaya, V.; Heine, T.; Seifert, G.; Wiesel, I.; Wagner, H. D.; Tenne, R. *Proc. Natl. Acad. Sci. U.S.A.* **2006**, *103* (3), 523−528.

Supporting Information for

Elastic Properties of Chemical-Vapor-Deposited Monolayer MoS_2, WS_2, and Their Bilayer Heterostructures

Kai Liu,[†,‡] *Qimin Yan,*[§,∥] *Michelle Chen,*[†] *Wen Fan,*[†,⊥] *Yinghui Sun,*[∥] *Joonki Suh,*[†] *Deyi Fu,*[†] *Sangwook Lee,*[†] *Jian Zhou,*[†] *Sefaattin Tongay,*[†] *Jie Ji,*[⊥] *Jeffrey B. Neaton,*[§,∥,◊] *Junqiao Wu*[*,†,‡]

[†]Department of Materials Science and Engineering, University of California, Berkeley, California 94720, United States

[‡]Materials Sciences Division and [§]Molecular Foundry, Lawrence Berkeley National Laboratory, Berkeley, California 94720, United States

[∥]Department of Physics and [◊]Kavli Energy Nanosciences Institute, University of California, Berkeley, California 94720, United States

[⊥]Department of Thermal Science and Energy Engineering, University of Science and Technology of China, Anhui 230027, China

*Corresponding author. Email: wuj@berkeley.edu

1. Transfer process of monolayer MoS_2 and WS_2

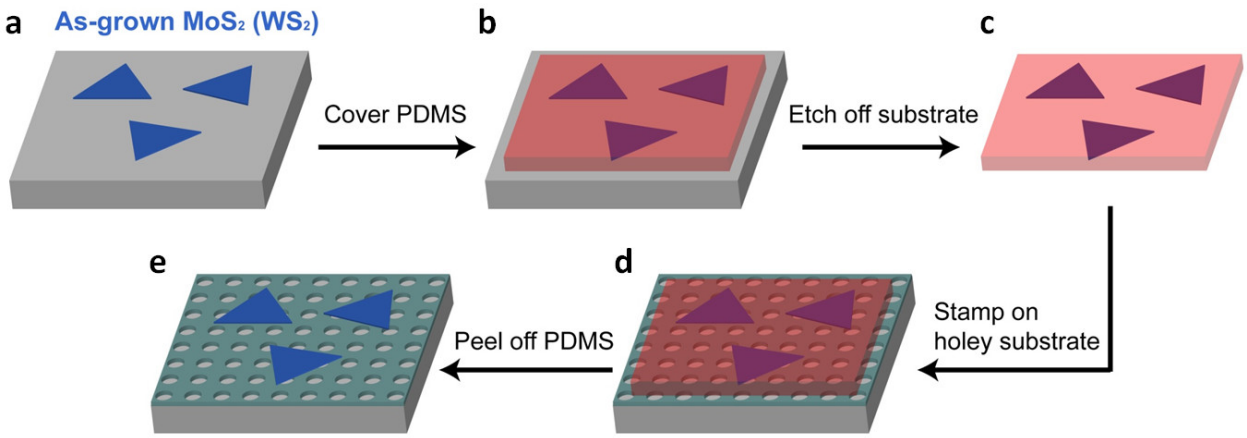

Figure S1. PDMS stamp of chemical-vapor-deposited 2D monolayers.

2. MoS_2 monolayers transferred on a holey substrate

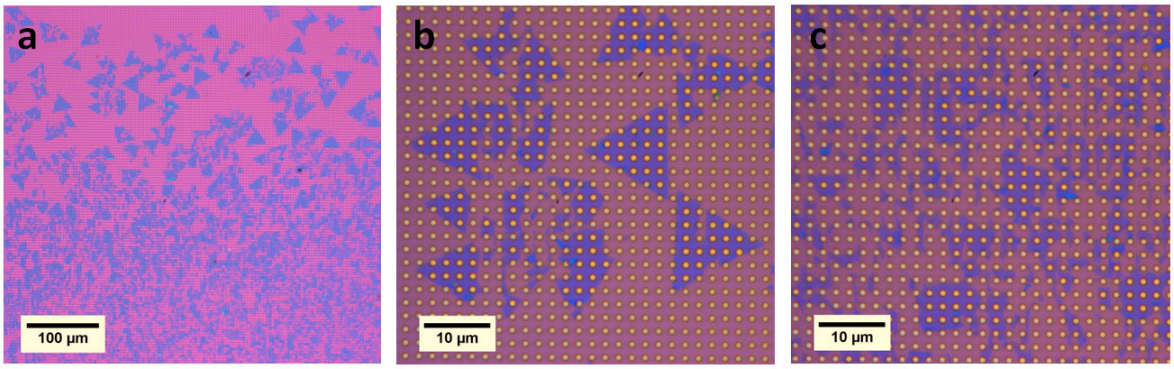

Figure S2. (a) Overall view of both isolated triangles and continuous part as grown on substrate. (b) Isolated triangle monolayers transferred onto the holey substrate. It shows most of triangles are transferred, and many of them are intact after the transfer. (c) Continuous monolayer part after transfer. The originally continuous film breaks into isolated pieces. The transfer yield is ~70 % in area for the triangle part and ~ 20 % for the continuous part. On a flat SiO_2/Si substrate, in contrast, almost 100% of triangle and continuous parts can be transferred.

3. Comparison of isolated and continuous parts of CVD MoS_2 monolayers

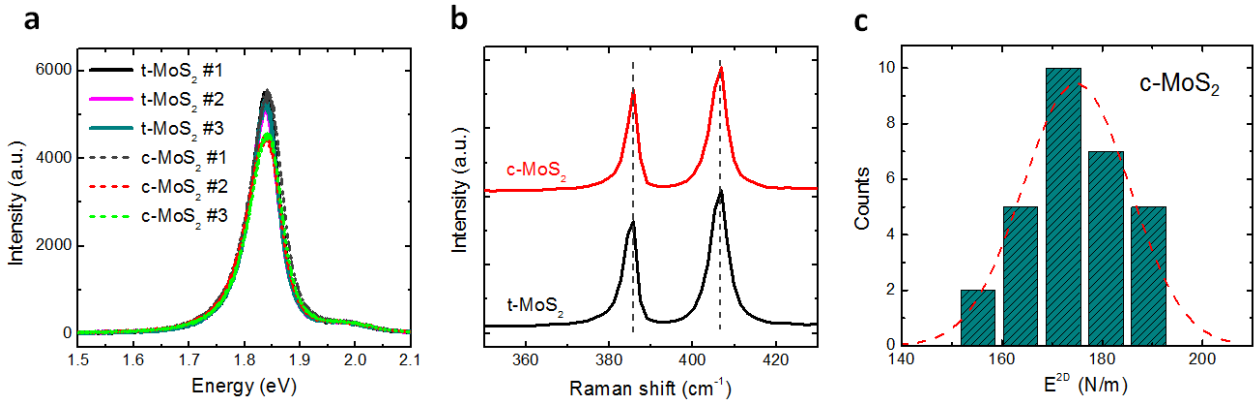

Figure S3. (a) Photoluminescence of triangle (t-MoS_2) and continuous (c-MoS_2) parts. Three different positions were probed for either part. (b) Raman spectra of both parts. (c) Statistical histogram of the 2D modulus of the continuous part of MoS_2. The very similar PL and Raman spectra, as well as the nearly identical modulus (171 ± 11 N/m for t-MoS_2 and 174 ± 10 N/m for c-MoS_2), suggest that these two monolayer parts have similar crystal quality.

4. As-grown and as-transferred WS_2

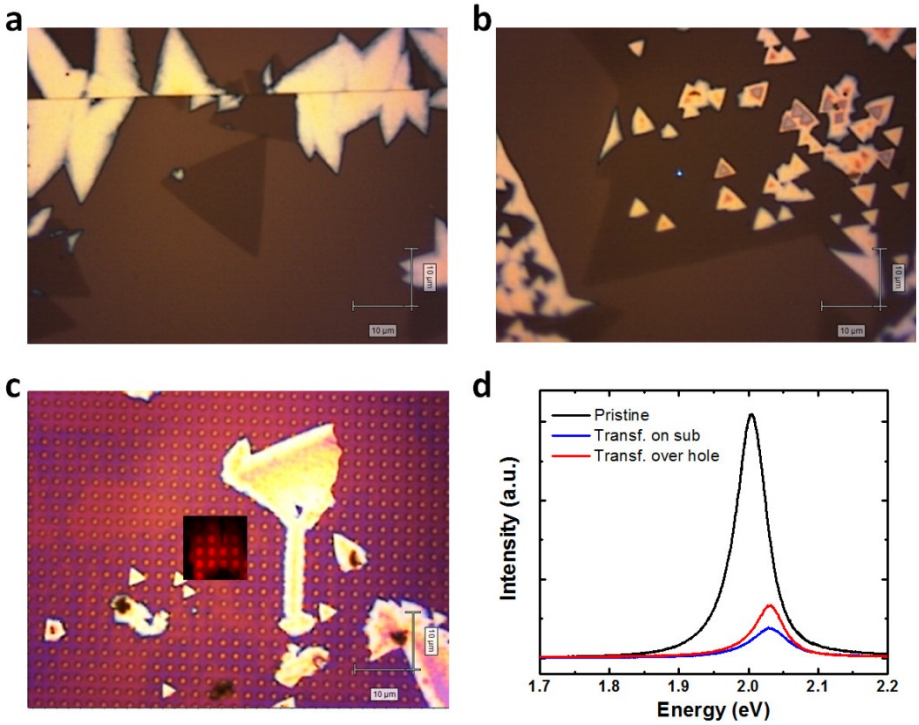

Figure S4. (a, b) Optical images of as-grown WS_2 sample. CVD WS_2 sample also has isolated triangles and relatively continuous part, but many thick WS_2 parts (bright color in images) form around the triangle and continuous parts, which is different from MoS_2 growth. (c) As-transferred WS_2 monolayer on a holey substrate. The inset shows PL mapping of the corresponding area. The suspended circular membranes present stronger PL intensities, which is the same as those of MoS_2. (d) PL spectra of as-grown and as-transferred WS_2. The as-grown WS_2 exhibits a PL peak at 2.00 eV originating from the A excitonic transition,[1, 2] while after transfer, this peak is blue shifted to 2.03 eV. This trend is similar to that of MoS_2 shown in Fig. 1g.

5. MoS_2/WS_2 heterostructure

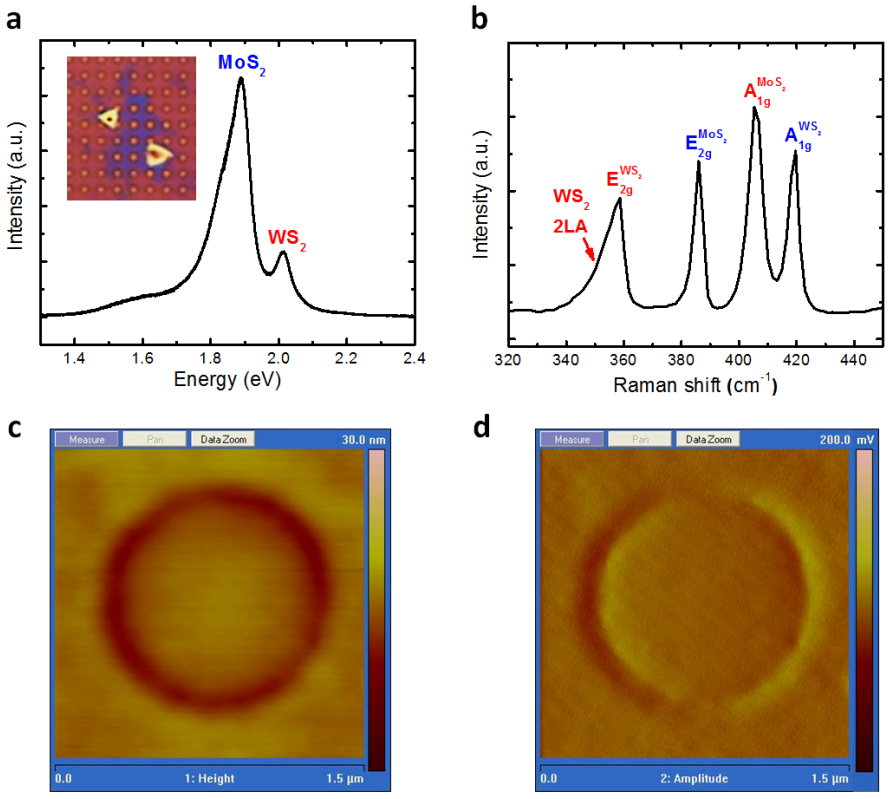

Figure S5. (a) PL spectrum of a suspended MoS_2/WS_2 hetero membrane in the area shown in the inset, demonstrating the overlap of PL peaks from direct band gap transitions of MoS_2 and WS_2. MoS_2/WS_2 heterostructure was fabricated by a two-step stamping transfer of firstly WS_2 and then MoS_2. We found that the second-step stamp peeled off some WS_2 monolayers that are previously transferred on the holey substrate, but also overlapped MoS_2 to WS_2 in some areas. (b) Raman spectrum of as-fabricated MoS_2/WS_2, also showing the combination of both Raman features.[3, 4] (c,d) AFM topology and amplitude images of a MoS_2/WS_2 hetero membrane, which do not show any bubbles or wrinkles on the substrate or over the hole.

6. Exfoliated MoS_2 bilayer

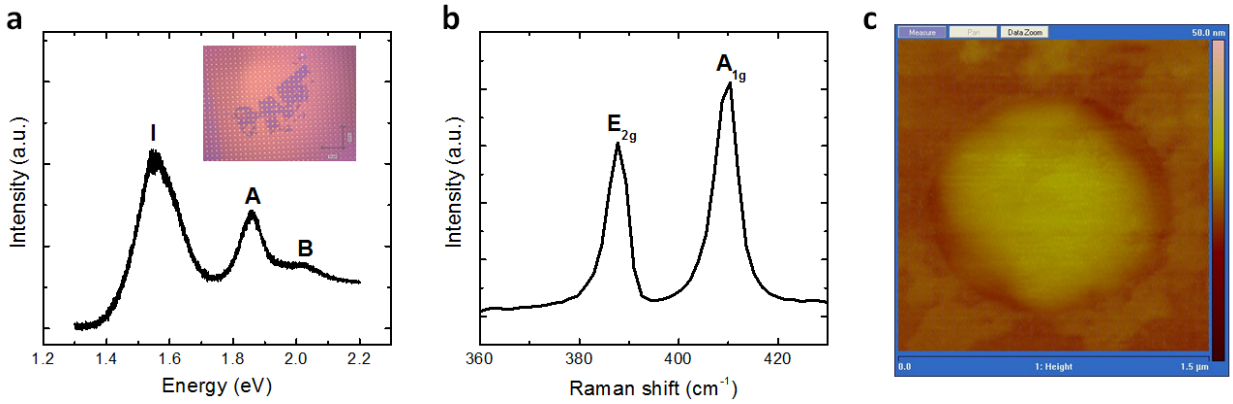

Figure S6. (a) PL spectrum of an exfoliated MoS_2 bilayer shown in the inset. The spectrum presents peaks of A and B excitonic transitions (centered at 1.86 eV and 2.03 eV, respectively), and indirect band gap transition, I (centered at 1.55 eV). (b) Raman spectrum of MoS_2 bilayer. The interval between E_{2g} and A_{1g} is 22 cm^{-1}. Both the PL and the Raman spectra match that of MoS_2 bilayer reported in literature.[3, 5] (c) AFM topology image of a MoS_2 bilayer membrane.

7. MoS_2/graphene heterostructure

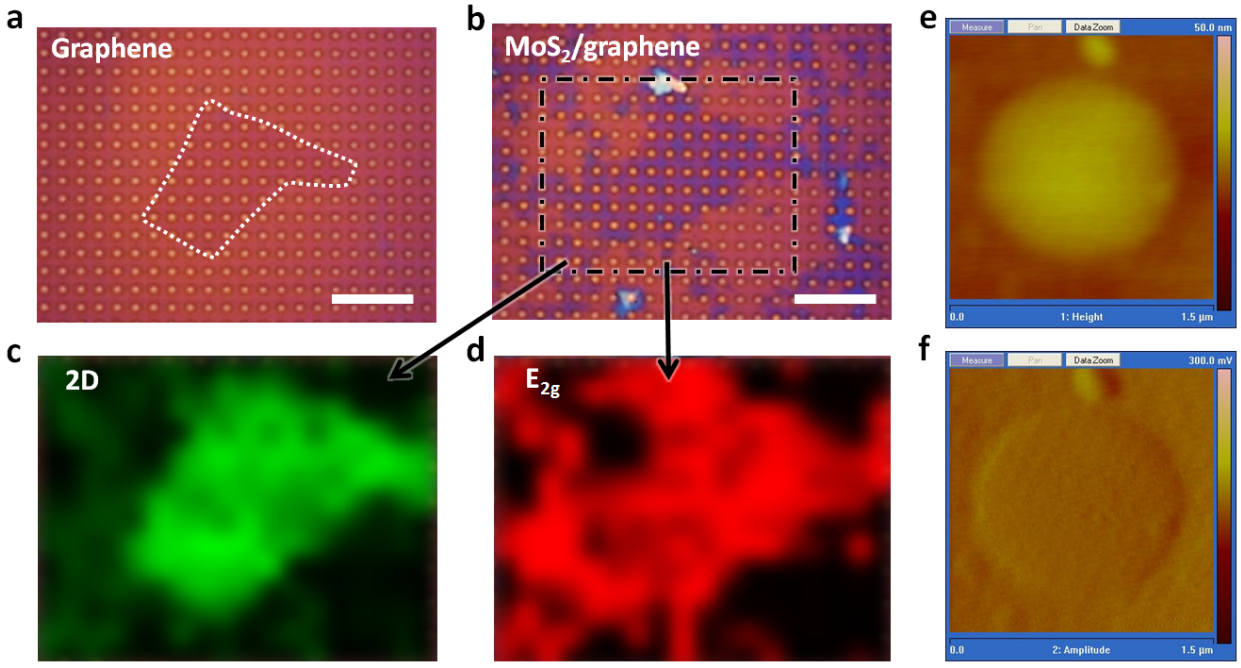

Figure S7. (a) As-exfoliated graphene on a holey substrate. The white dotted line shows the edge of the graphene monolayer. (b) Transfer of CVD MoS_2 by PDMS stamp, overlapping MoS_2 continuous monolayer on graphene and forming MoS_2/graphene heterostructure. The area labeled by black dash-dot line is mapped in Raman spectra. (c) Raman mapping of 2D peak (2692 cm^{-1}), showing the area of graphene. (d) Raman mapping of E_{2g} peak (387 cm^{-1}), showing the area of MoS_2. (e and f) AFM topology and amplitude images of a MoS_2/graphene hetero membrane. No evidence of bubbles or wrinkles exists on the substrate or over the hole.

8. Model for the calculation of elastic properties of MoS_2 and WS_2

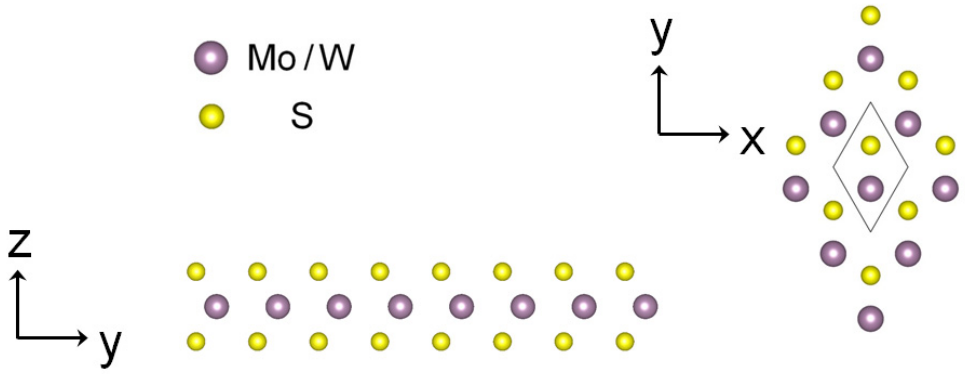

Figure S8. Top (right) and side view (bottom) of monolayer MoS_2 or WS_2. The unit cell used in our simulations is marked by the black diamond box. Two in-plane directions (x and y) are represented by the arrows.

9. E^{2D} at various indentation depths

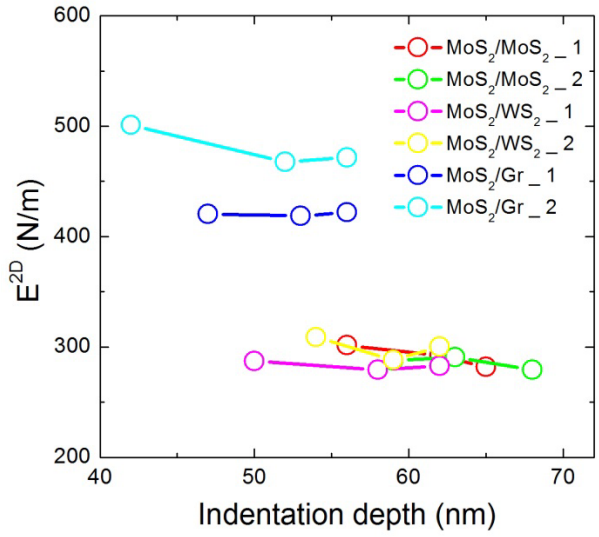

Figure S9. Measured E^{2D} at various indentation depths for different bilayer structures. Two membranes of each type of bilayer structures were measured and plotted. There is no evident dependence of E^{2D} on the indentation depth within the experimental error.

References

1. Zhao, W. J.; Ghorannevis, Z.; Chu, L. Q.; Toh, M. L.; Kloc, C.; Tan, P. H.; Eda, G. *Acs Nano* **2013,** 7, (1), 791-797.
2. Gutierrez, H. R.; Perea-Lopez, N.; Elias, A. L.; Berkdemir, A.; Wang, B.; Lv, R.; Lopez-Urias, F.; Crespi, V. H.; Terrones, H.; Terrones, M. *Nano Letters* **2013,** 13, (8), 3447-3454.
3. Lee, C.; Yan, H.; Brus, L. E.; Heinz, T. F.; Hone, J.; Ryu, S. *Acs Nano* **2010,** 4, (5), 2695-2700.
4. Berkdemir, A.; Gutiérrez, H. R.; Botello-Méndez, A. R.; Perea-López, N.; Elías, A. L.; Chia, C.-I.; Wang, B.; Crespi, V. H.; López-Urías, F.; Charlier, J.-C.; Terrones, H.; Terrones, M. *Scientific Reports* **2013,** 3.
5. Mak, K. F.; Lee, C.; Hone, J.; Shan, J.; Heinz, T. F. *Phys. Rev. Lett.* **2010,** 105, (13), 4.